Extracellular mycobacterial DNA triggers Caspase-11-dependent pyroptosis of infected macrophages and drives disease progression

Monica Varela[1], Michiel van der Vaart[1], Arwin Groenewoud[1] and Annemarie H. Meijer[1]

Affiliations

[1]Institute of Biology Leiden; Leiden University; Leiden, 2233CC; The Netherlands

Correspondence:

Annemarie H. Meijer: a.h.meijer@biology.leidenuniv.nl

Monica Varela: m.varela.alvarez@biology.leidenuniv.nl

Keywords

Caspase-11, Gasdermin D, Inflammasome, Pyroptosis, extracellular DNA, Cell-in-cell, Mycobacterium, Zebrafish, Macrophage, Granuloma, Tuberculosis

SUMMARY

Deregulated inflammation is a serious complication of life-threatening microbial infections, including tuberculosis (TB). The pathological hallmark of TB, the granuloma, is an inflammatory structure crucial for containing infection. However, excessive inflammation in granulomas can cause tissue damage and promote bacterial proliferation and dissemination. The assembly of multiprotein inflammasome complexes is an important trigger of inflammation, but it remains unknown how inflammasome activation impacts TB granuloma progression. Here, by *in vivo* imaging using the zebrafish TB model, we found that inflammasomes and ensuing pyroptotic cell death of infected macrophages drive granuloma expansion and disease progression. We show that different types of inflammasomes are activated during granuloma formation, with host-protective roles for Asc-dependent inflammasome activation and Il1b secretion. In contrast, an Asc-independent pathway induces macrophage pyroptosis and impairs host resistance. Complementary research in ASC-deficient murine macrophages reveals that extracellular bacterial DNA induces CASP11-dependent pyroptosis in a manner dependent on phagosome permeabilization. Finally, we show that mycobacteria induce pyroptosis to escape from cell-in-cell structures that form within granulomas when living infected cells are engulfed by newly attracted macrophages. This study provides new insights into the role of pyroptosis in TB pathogenesis and unravels a novel link between nucleic acid sensing and CASP11-dependent pyroptosis.

INTRODUCTION

Mycobacterium tuberculosis (*Mtb*), the causative agent of tuberculosis (TB), has developed many strategies to manipulate the host immune response (Lerner et al., 2015, Liu et al., 2017). The successful establishment of the infection depends on the early interactions between pathogen and host innate immune cells, especially macrophages (Sia et al., 2015). Macrophages play a central role in TB pathogenesis and are the principal niche for intracellular growth of *Mtb* or closely related mycobacterial pathogens, including *Mycobacterium marinum* (*Mmar*), which causes TB in cold-blooded animals (McClean et al, 2016).

Granulomas, considered as the pathological hallmark of TB, are inflammatory cell structures, rich in macrophages. Granuloma formation starts with aggregation of mycobacterium-infected macrophages and subsequent recruitment of uninfected macrophages. These early stages of granuloma formation favor spreading of bacteria from cell to cell and are dependent on the bacterial RD1 (ESX1) virulence locus (Ramakrishnan, 2012). At later stages, T-cells and other immune cells are attracted, which are essential to contain the infection. Therefore, granulomas have a dual role, on the one hand serving a host-protective function, but on the other hand enabling dissemination and long-term survival of the pathogen inside its host. Because the failure of one granuloma to control infection can already be sufficient to initiate disease progression (Cadena et al., 2017), a better understanding of granuloma function is of crucial importance. Many studies have shown that the local balance of pro- and anti-inflammatory responses is critical for determining the fate of individual granulomas and the final disease outcome (Mayer-Barber et al., 2010; Marakalala et al., 2016). However, the molecular mechanisms that drive inflammation in the granuloma remain to be elucidated.

The inflammasomes are multiprotein signaling platforms that allow the activation of inflammatory caspases (caspase-1, -4, -5, -11) in response to infections and endogenous danger signals (Martinon et al., 2002; Latz et al., 2013; Broz and Dixit, 2016; Russo et al., 2018). Activation of cytosolic pattern recognition receptors that are contained within canonical inflammasomes promotes activation of caspase-1 (CASP1) and interleukin-1β (IL1β) maturation (Afonina et al., 2015). In contrast, the non-canonical inflammasome is dependent on murine Caspase-11 (CASP11) or human Caspase-4/5 (CASP4/5) (Kayagaki et al., 2011). In response to several Gram-negative pathogens, CASP11 mediates mouse macrophage death via direct interaction with LPS (Shi et al., 2014; Yang et al., 2015). Both inflammasome types activate gasdermin D (GSDMD), which is the executioner of pyroptotic cell death by forming pores in cell membranes (Kayagaki et al., 2015; Shi et al., 2015). Due to the recognition of its necrotic nature, pyroptosis has recently been redefined as gasdermin-mediated programmed necrotic cell death (Shi et al., 2017).

Despite the known occurrence of necrotic cell death within TB granulomas (Grosset, J., 2003), the role of pyroptosis in granuloma formation and expansion remains unexplored. The well-established zebrafish TB model has been a very useful

tool in the study of the disease as it recapitulates many aspects of human tuberculous granulomas (Davis et al., 2002; Ramakrishnan, 2012; Cronan et al., 2016; Meijer, 2016). Studies in zebrafish have shown that granuloma expansion is driven by cell death and subsequent efferocytosis of infected macrophages and that uncontrolled extracellular proliferation of mycobacteria occurs under experimental conditions that promote necrotic rather than apoptotic forms of macrophage cell death (Davis and Ramakrishnan, 2009; Roca et al., 2013; Pagan et al., 2015). New tools recently developed for the study of inflammasomes (Kuri et al., 2017) make zebrafish a suitable model for *in vivo* visualization of inflammasomes activation and investigation of the role of pyroptosis in granuloma formation.

Here, we report that different inflammasome pathways are activated in infected macrophages during mycobacterial infection. While a pathway dependent on the adaptor protein ASC promotes resistance of the zebrafish host to TB infection, we find that a CASP11 homologous pathway promotes pyroptotic cell death of infected macrophages and exacerbates infection. Using Raw264.7 macrophages, we subsequently showed that extracellular bacterial DNA triggers CASP11 activation and GSDMD-dependent pyroptosis, revealing a novel link between nucleic acid sensing and non-canonical inflammasome activation. Finally, we identified the formation of cell-in-cell structures within developing granulomas and demonstrated that *Mmar)* is able to escape cell-in-cell structures by triggering pyroptosis, thereby initiating in this way its dissemination and promoting disease progression.

RESULTS

1. Asc and Il1b are host-beneficial during *Mmar* infection in zebrafish

The interleukin 1 signaling pathway is known to be critical for immunity against tuberculosis (Mayer-Barber et al., 2010; Bohrer et al., 2018; Cohen et al., 2018). To evaluate the role of this pro-inflammatory cytokine in the zebrafish TB model, we transiently knocked-down *il1b* in zebrafish larvae. After 2 days of infection, an increased bacterial burden in knockdown fish was observed (**Figure 1A and S1A**), suggesting that Il1b is host-protective during *Mmar* infection in this model. In macrophages, maturation and secretion of IL1β occur after activation of inflammasomes (Latz et al., 2013). For signaling, most of the known inflammasomes require an adaptor molecule, ASC (reviewed in Palazón-Riquelme and Castejón, 2018). Knockdown (KD) of *asc* increased *Mmar* burden in zebrafish larvae (**Figure 1B and S1B**). We next investigated ASC oligomerization, considered a hallmark of inflammasome activation. Formation of ASC specks can be visualized just before pyroptosis occurs (Miao et al., 2011). *In vivo* imaging of zebrafish granulomas showed macrophage pyroptosis occurring after the formation of Asc specks (**Figure 1C**). Typically, only one speck per granuloma was observed at a time (**Figure S1C**). In contrast, Asc speck-independent cell death was more often observed in granulomas (**Figure S1D**). After pyroptosis, as Kuri et al. (2017) showed before, Asc specks can be engulfed and degraded by neighboring macrophages (**Figure 1D and 1SE; Movie 1).**

2. Two inflammasome signaling axes are differentially regulated upon *Mmar* infection

Next, we decided to investigate the role of inflammatory caspases, such as CASP1/4/5/11, indispensable in ASC-dependent and -independent inflammasome signaling pathways (Man et al., 2017). Because zebrafish Caspa and Caspb have been traditionally considered CASP1 functional homologues as they can process IL1β *in vitro* (Vojtech et al., 2012), we determined the effect of *caspa* and *caspb* transient KD in *Mmar* infected zebrafish. Surprisingly, Caspa and Caspb deficiency resulted in opposite bacterial burden outcomes, with *caspa* KD reducing infection and *caspb* KD increasing infection (**Figure 2A, 2B, S2A, S2B and S2C**). Moreover, we found that the double KD of *caspa* with *caspb* or with *asc* resulted in the same reduced infection phenotype as single KD of *caspa* (**Figure 2C and S2D**). In addition, double KD of *caspb* with *asc* had no additive effects in terms of bacterial growth, suggesting that both genes are in the same pathway (**Figure S2D**). At a cellular level, we observed that while *caspb* KD increased *Mmar* extracellular growth, *caspa* KD was sufficient for restricting the infection (**Figure 2D**).

Recently, gasdermin D (GSDMD), which requires processing by inflammatory caspases to form pores in cell membranes, was identified as essential effector of pyroptosis (Kayagaki et al., 2015; Shi et al., 2015). In the zebrafish genome, two

proteins with GSDM domain can be identified, Gsdmea and Gsdmeb. *In silico* predictions show that Gsdmeb has a CASP1 cleavage site, which is also the case for GSDMD (**Figure S2E**). Because of this similarity, we knocked-down *gsdmeb* in zebrafish larvae (**Figure S2F and S2G**). The lack of Gsdmeb resulted in decreased *Mmar* burden 2 days after infection. In addition, the combination of *gsdmeb* KD with *caspa* deficiency had no additive effects (**Figure S2H**).

Taken together, the results above suggest the involvement of at least two inflammasome pathways during the course of *Mmar* infection, namely a host-protective Asc-Caspb-Il1β axis and a host-detrimental Caspa-Gsdmeb axis (**Figure 2E**). This observed duality prompted us to further investigate the functional homology of the zebrafish inflammatory caspases and their murine counterparts. For this, overexpression of zebrafish *caspa* and *caspb*, and murine *Casp1* and *Casp11* mRNAs in *caspa*$^{-/-}$ zebrafish was performed (**Figure 2F**). In terms of bacterial burden, only zebrafish *caspa* and murine *Casp11* mRNAs were able to fully rescue the *caspa* mutant phenotype, demonstrating that Casp11 can compensate for the loss-of-function of Caspa and suggesting that in the context of *Mmar* infection the host-detrimental Caspa-Gsdmeb axis in zebrafish is equivalent to the mammalian Casp11-Gsdmd pathway.

3. *Mmar* triggers ASC-independent cell death after phagosomal membrane rupture

To fully understand the dynamics of inflammasome activation in zebrafish, we explored the formation of ASC specks in the granuloma in combination with *in situ* caspase activity detection, using a fluorescently labeled inhibitory substrate (Flica YVAD) specific for zebrafish Caspa (Masumoto et al., 2003). As observed earlier, Asc specks appeared in close contact with bacterial clusters (**Figure 3A).** *In situ* staining revealed that active Caspa was abundant in granulomas, visible either in small specks or in patchy patterns around *Mmar* **(Figure 3A, S3A and S3B**). We found that Caspa activation occurred in Asc specks and, in an Asc-independent manner, in both Caspa specks and patches (**Figure 3B and S3C)**. We next assessed whether ASC is required for induction of macrophage pyroptosis *in vitro* after *Mmar* infection (**Figure 3C**). Using ASC-deficient Raw264.7 macrophages (Pelegrin et al., 2008) we observed pyroptosis occurring 16 minutes after bacterial phagosome rupture (**Figure 3D, Movie 2**). To confirm the role of phagosomal rupture in the induction of pyroptosis we used mutant *Mmar* lacking the RD1 virulence locus. We found that *Mmar* ΔRD1 could not induce pyroptosis in Raw264.7 macrophages (**Figure 3E**). To further demonstrate the importance of phagosomal membrane rupture in the dissemination of infection we compared bacterial burdens in zebrafish after infection with *Mmar* ΔRD1 in *caspa* KD conditions (**Figure 3F**). We found that Caspa deficiency had no effect on bacterial burden when bacteria were not able to escape the phagosome, suggesting that phagosomal membrane permeabilization is required for Caspa activation and ensuing pyroptotic cell death.

4. *Mmar* infection triggers Caspase-11 and Gasdermin D-dependent pyroptosis

A previous report showed that CASP1 was not required for *Mtb*-induced cell death in primary mice macrophages (Lee et al., 2011). Because our zebrafish data implicated CASP11 in the dissemination of *Mmar* infection, we asked whether or not pyroptosis is CASP11 dependent in murine macrophages. CASP11 cleavage was detected in the supernatant of Raw264.7 macrophages infected with WT *Mmar* (**Figure 4A, S4A**). In contrast, CASP11 was not processed upon *Mmar* ΔRD1 infection. In agreement, infection with WT *Mmar* led to high levels of LDH release, while the lack of LDH release after infection with *Mmar* ΔRD1 indicated that cell death was not induced (**Figure 4B**). Additionally, knockdown of *Casp11* and *Gsdmd* in Raw264.7 macrophages diminished Mmar-induced cell death (**Figure 4C, S4B**). Having demonstrated the importance of CASP11 and GSDMD-dependent cell death *in vitro*, we next investigated its role *in vivo*. Numbers of TUNEL-positive cells were reduced following *caspa* and *gsdmeb* KD in *Mmar*-infected zebrafish (**Figure 4D and 4E**). In conclusion, both *in vitro* and *in vivo* data support the requirement of CASP11/Caspa and GSDMD/Gsdmeb for *Mmar*-dependent pyroptotic cell death.

5. Mycobacterial extracellular DNA triggers Caspase-11 and Gasdermin D-dependent pyroptosis of infected cells

We next sought to identify the bacterial component that induces CASP11 cleavage and GSDMD-dependent pyroptosis of infected macrophages. Unexpectedly, while investigating cell death during infection in zebrafish, we frequently observed positive TUNEL staining other than cell nuclei around *Mmar* (**Figure 5A**). To identify the source of this DNA we stained the bacterial culture with the DNA dye Draq5 prior to the infection of Raw264.7 macrophages (**Figure 5B**). During infection, we observed Draq5-positive DNA around *Mmar* while the cell nuclei remained negative, indicating the bacterial origin of this DNA. To explore the possible involvement of such extracellular bacterial DNA in pyroptosis induction, we simulated this situation by coating *Mmar* with ultrapure *E. coli (Ec)* genomic DNA (gDNA) (**Figure 5C**), endotoxin-free *Mmar* genomic DNA, CpG oligonucleotides (ODN2395), and *Ec* LPS as known CASP11 activator. We found that LPS and both *Mmar* and *Ec* genomic DNAs, but not ODN2395, were able to increase pyroptosis of Raw264.7 macrophages (**Figure 5D**). This effect was not observed during infection with *Mmar* ΔRD1, consistent with the inability of this strain to induce phagosome rupture (**Figure 5E**). Importantly, we found that cell death induced by extracellular bacterial DNA is CASP11 and GSDMD-dependent (**Figure 5F**).

6. Granuloma formation and *Mmar* dissemination *in vivo* is related to the bacterial ability to trigger Caspase-a activation and block phagosome acidification

In vivo, proliferation of *Mmar* is related to its ability to escape from phagosomes and induce granuloma formation (**Figure 6A and 6B**). The inability of *Mmar* ΔRD1 to form typical mycobacterial granulomas and trigger Caspa activation (**Figure 6C**), suggests that Caspa activation is required for *Mmar* dissemination *in vivo*. Indeed, active Caspa was highly detected in granuloma cells (**Figure 6D**).

In recent years, inflammasomes have been associated with phagosome acidification and maturation during infection (Sokolovska et al., 2013). To investigate the possible implication of Caspa in the maturation of *Mmar*-containing phagosomes we analyzed *in situ* Caspa activation in relation to acidification of organelles using LysoTracker (LT) staining. We observed that some bacterial clusters within the granuloma are Flica+ve but LT-ve, which can be interpreted as Caspa activation preceding or preventing phagosome acidification (**Figure 6E**). In line with this, we found that the lack of Caspa alters the acidification pattern of bacterial containing vesicles (**Figure 6F**). Acidic vesicles accumulated around *Mmar* but did not colocalize with bacteria in wildtype fish, however, in absence of Caspa, LT staining and *Mmar* fully colocalized (**Figure 6F**). These results suggest that the ability of *Mmar* to block phagosome maturation is dependent on the activation of Caspa in the infected host cell. Moreover, the investigation of *Mmar*-LT colocalization in granulomas revealed the presence of LT patterns concentrically surrounding *Mmar* clusters. Because such lysosomal ring patterns are a known cytological feature of entosis (Garanina et al., 2015), this observation suggests the presence of cell-in-cell structures in mycobacterial granulomas (**Figure 6G**).

7. *Mmar* elicits pyroptosis to escape cell-in-cell structures in granulomas

We next decided to investigate the role of cell-in-cell structures in the fate of the infection. The presence of cell-in-cell structures in granulomas is made visible using cytoplasmic ASC as cell marker that allows visualizing the entotic vacuole between inner and outer cells devoid of cytoplasmic material. While inner cells are always infected, this is not the case for the outer cell that engulfed the infected inner cells (**Figure 7A and S5A**). We observed the formation of such multinucleated cell structures *in vivo* (**Figure 7B and S5B**) and *in vitro* during the course of *Mma*r infection (**Figure S5C and movie 3**). Time-lapse analysis revealed cell-cell contacts occurring before cell invasion. Moreover, we observed how the outer cell transfers bacteria into an inner cell (**Figure S5C and movie 3)**. Taken together, these results suggest an active role for the outer cell, most likely as a consequence of the cell-cell communication happening before engulfment.

Several mechanisms have been described where the engulfment of whole live cells, leading to the formation of cell-in-cell structures, induces cell death (Krishna and Overholtzer, 2016). In *Mmar* granulomas we observed engulfment of infected macrophages (Asc+ve, Mpeg1+ve) and their degradation inside outer cells, in this case, an epithelial cell in this case (Asc+ve, Mpeg1-ve) (**Figure 7C**). Besides a role for cell

engulfment mechanisms in killing inner cells, we observed the expulsion of infected inner cells in granulomas (**Figure 7D and S5D; movie 4**). This regurgitation follows the initiation of the pyroptotic cell death program of the inner cell, which in some occasions resulted in pyroptotic dead of both the inner and outer cell (**Figure 7E and S5E; movie 5**). Importantly, pyroptosis of infected cells was host-detrimental as *Mmar* was subsequently able to proliferate and expand the extracellular infection foci (**Figure S6A**). We observed that extracellular *Mmar* attracts new phagocytic cells to the area, which die via pyroptosis shortly after phagocytosis, thereby functioning as a mechanism for rapid expansion of the infection (**Figure S6B; movie 6**). Based on these results, we conclude that pyroptosis of internalized infected cells during entosis in granulomas favors *Mmar* survival and dissemination.

DISCUSSION

Inflammasome signaling is central to many anti-bacterial host responses. Specifically, CASP11 and its human othologues CASP4 and CASP5 are emerging as key regulators of this pathway, but their involvement in pathological inflammation during TB remains unexplored. Based on *in vitro* data in murine macrophages and *in vivo* data in zebrafish larvae, we propose CASP11/Caspa as a critical mediator of the dissemination of mycobacterial infection. We found that phagosome permeabilization is required for induction of CASP11/Caspa and GSDMD/Gsdmeb-dependent pyroptosis in response to bacterial eDNA. Furthermore, *Mmar* directs the activation of CASP11/Caspa-dependent pyroptosis to escape cell-in-cell structures in granulomas. Together, these findings unravel a mechanism exploited by the bacteria to survive and disseminate within the host.

In agreement with recent reports on macrophages *in vitro* (Evavold et al., 2018; Monteleone et al., 2018), our data suggest that Il1b processing and pyroptosis might be uncoupled during *Mmar* infection in zebrafish. Deregulated production of IL1β worsens TB and therefore it needs to be tightly regulated in the course of the disease (Mayer-Barber et al., 2010; Mayer-Barber et al., 2011, Boher et al., 2018). In our model, IL1b processing seems to occur mainly downstream of an Asc-dependent inflammasome and the host-protective function of this pathway is supported by increased infection burden under both *il1b* and *asc* knockdown conditions. ASC aggregates are stable and can trigger prolonged inflammation even when they are released to the extracellular space (Baroja-Mazo et al., 2014; Franklin et al., 2014). In this regard, the host might be able to regulate the number of specks forming to avoid an excessive and detrimental inflammatory response within the granuloma. Due to the highly inflammatory nature of TB in its active state (disseminated tuberculosis), a comparison with sepsis is of interest. Both *Gsdmd*$^{-/-}$ and *Casp11*$^{-/-}$ mice survive after a challenge with lethal doses of LPS (Kayagaki et al., 2015; Shi et al., 2015). In line with this, our data show that CASP11/Caspa and GSDMD/Gsdmeb activation is host-detrimental *in vitro* and *in vivo* during *Mmar* infection. It remains to be established if CASP11 and GSDMD have similar disease exacerbating roles during infection with *Mtb*.

We found that macrophage pyroptosis requires phagosome permeabilization which was directly related to the ability of *Mmar* to activate CASP11/Caspa as *Mmar* lacking the RD1 locus/ESX-1 system cannot activate CASP11/Caspa. ESX-1 is responsible for translocation of eDNA to the cytosol during mycobacterial infections (Stanley et al., 2007; Manzanillo et al., 2012). We observed that genomic DNA from *Mmar* and *Ec* can activate pyroptosis *in vitro* in a CASP11-GSDMD-dependent manner in the same magnitude as LPS. CASP11 can bind directly to intracellular LPS, resulting in CASP11 processing and activation (Shi et al., 2014), but whether a direct interaction between eDNA and CASP11/Caspa also exists will require further research. Recent studies reveal a novel function for guanylate-binding proteins (GBPs) in controlling the intracellular detection of LPS derived from extracellular bacteria in the form of outer membrane vesicles (Santos et al., 2017). Moreover, in response to certain cytosolic

bacteria, GBPs liberate microbial DNA for activation of the DNA-sensing AIM2 inflammasome (reviewed in Man et al., 2017). Intriguingly, the AIM2 inflammasome is an ASC-dependent inflammasome, indicating that CASP11 activation in ASC-deficient Raw264.7 macrophages upon *Mmar* infection must occur via a different pathway. Secretion of eDNA has recently been proposed as a pro-survival strategy in bacterial communities (Vorkapic et al., 2016). The architecture of these communities depends on the production of an extracellular matrix, of which DNA is part (Flemming et al., 2016). Interestingly, most of the known mechanisms of eDNA release are regulated by quorum sensing, and therefore eDNA is usually produced in response to an increase in the cell density of the population (Ibáñez de Alcoa et al., 2017). In mycobacteria, stress and quorum sensing result in the formation of biofilm-like structures and persistent cells in necrotic areas (Basaraba, 2008), suggesting that eDNA secretion is not only host-detrimental because of its ability to induce pyroptosis of infected cells but also because it can facilitate extracellular proliferation of bacteria.

Notably, we identified cell-in-cell structures in *Mmar* granulomas. Cell-in-cell structures were described decades ago, but their biological significance is only just beginning to be unraveled. Within the last few years, several forms of cell-in-cell death have been described, among which entosis and cannibalism are of special interest in cancer research and tumor prognosis (Fais and Overholtzer, 2018). The main difference between these two processes is the cell taking the lead during engulfment. During cell cannibalism the outer cell leads and engulfs inner cells, while during entosis, is the inner cell that pushes itself into the outer cell (Yang and Li, 2012). Besides the differences, both processes end in lysosomal digestion of inner cells (Fais, 2007; Overholtzer et al., 2007). Regulated by nutrient signaling pathways, entosis is induced under starvation conditions (Hamann et al., 2017). In the context of *Mmar* infection, degradation of inner cells is visible within granulomas, but it remains to be explored whether this mechanism is involved in acquisition of cell nutrients or is primarily a measure of infection containment. One other infection study has previously reported on cell-in-cell structures, revealing that Epstein-Barr virus uses an in-cell infection mechanism to spread from infected B cells to epithelial cells (Ni et al., 2015).

Granuloma macrophages can undergo multinucleated giant cell (MGC) formation or epithelioid transformation and epithelial cadherin (E-cadherin) has been proposed as a common link between these two differentiation pathways (Pagan et al., 2018). Interestingly, entosis is induced by the expression of E-cadherin proteins (Sun et al., 2014), pointing to the possible implication of entosis in forming MGCs in granulomas. In zebrafish, macrophage-specific disruption of E-cadherin function resulted in disordered granuloma formation, enhanced immune cell access, decreased bacterial burden, and increased host survival (Cronan et al., 2016). This would suggest that the formation of cell-in-cell structures in granulomas, if dependent on E-cadherin, could be pathogen-protective. The fates of the innner cells and outer cells in cell-in-cell structures are diverse (Overholtzer and Brugge, 2008). Our data demonstrate that pyroptosis is induced by virulent *Mmar* in inner cells to escape cell-in-cell structures in

granulomas, thereby contributing to the expansion of granulomas and infection progression. How pyroptosis induction occurs in the context of cell-in-cell structures will be the focus of future research. If CASP11/Caspa is involved in delaying phagosome maturation, it may also be implicated in delaying lysosomal degradation of inner cells. In this regard, the inner cell could be considered like a big phagosome inside the outer cell (a matryoshka doll-like or nested structure) and the same mechanisms implicated in inner cells releasing could be responsible of phagosome permeabilization.

Overall, these findings highlight the importance of cell-cell interactions in TB pathogenesis. Local inflammation, the immune response and bacterial state all contribute to the fate of a granuloma. Therefore, there are multiple pathways that can be manipulated to either control infection or promote bacterial dissemination. CASP11/Caspa-dependent pyroptosis increases bacterial survival and dissemination, not only allowing the bacteria to grow in the extracellular space but also increasing infection of new cells. We propose a central role for CASP11/Caspa in regulating bacterial phagosome degradation as well as mediating mycobacterial escape from cell-in-cell structures in granulomas. Based on these results, human CASP4/5 might be a valuable biomarker for monitoring TB therapy and its role during infection should be taken into account for the design of new therapeutic interventions.

EXPERIMENTAL PROCEDURES

Zebrafish husbandry and infections

Zebrafish (*Danio rerio*) were handled in compliance with the directives of the local animal welfare committee of Leiden University (License number: 10612) and maintained according to the standard guidelines from the Zebrafish Model Organism Database (http://zfin.org). All protocols adhered to the international guidelines specified by the EU Animal Protection Directive 2010/63/EU. All zebrafish experiments were done on embryos or larvae up to 5 days post fertilization (hpf), which have not yet reached the free-feeding stage. Embryos were grown at 28.5ºC and kept under anesthesia with egg water containing 0.02% buffered 3-aminobenzoic acid ethyl ester (Tricaine, Sigma) during bacterial injections, imaging and fixation. The following zebrafish lines were used in this study: AB/TL, Tg(*mpeg1.1:mCherryF*), Tg(*asc:asc-EGFP*) (Kuri et al., 2017) and the mutant line *caspa*^{hdb11} (Kuri et al., 2017).

Mycobacterium marinum (*Mmar*), M and ΔRD1 strain, expressing mWasabi, mCherry or mCrimson, preparations were injected into 30 hpf zebrafish embryos via blood island injection following previously described methods (Benard et al., 2012). A total of 300 cfu of *Mmar* in a volume of 1nl were injected per embryo in all experiments performed in this study.

Morpholino oligonucleotides

Morpholino oligonucleotides (MO) were designed and synthesized by Gene Tools (Philomath, OR). Previously validated MO were used in this work: IL1b i2e3 (0,5 mM): 5´-CCCACAAACTGCAAAATATCAGCTT-3´ (Ogryzko et al., 2014), ASC atg (0,6 mM): 5´-GCTGCTCCTTGAAAGATTCCGCCAT-3´ (Kuri et al., 2017), CASPa atg (0,6 mM): 5´-GCCATGTTTAGCTCAGGGCGCTGAC-3´ (Masumoto et al., 2003). New MO were validated during this research: GSDMEb e2i2 (0,7 mM): 5´-TCATGCTCATGCTAGTCAGGGAGG-3´, CASPb e2i2 (0,5 mM): 5´-AATCAAAATACTTGCATCGTCTCCG-3´. This Mo were validated by PCR using the following primers: Caspb ex1 F: 5´-ATGGAGGATATTACCCAGCT-3´, Caspb ex7 R: 5´-TCACAGTCCAGGAAACAGGT-3´, GSDMEb ex1 F: 5´-CAAGCGTAACCGATACTGGT-3´, GSDMEb ex5 R: 5´-AATCCACCTTTGACTGCTGG-3´. Morpholinos were diluted in sterile water with 1% phenol red sodium salt solution (Sigma) and 1 nl of the above mentioned final concentration was injected into the cell of 1 cell-stage embryos.

Cell Culture and infections

The mouse macrophage-like cell line Raw264.7 was a gift from Dr. Sander van Kasteren. Cells were maintained in 50% Dulbecco´s modified Eagle´s medium

(DMEM) and 50% F12 medium with 10% fetal calf serum, at 32ºC under a humidified atmosphere of 94% air and 6% CO2.

For WB experiments cells were seeded in 6-well plates (Greiner) at a density of $2 \cdot 10^6$ cells/well the day before the infection. Cells were infected at a MOI of 10 for 2 hours at 32ºC. The extracellular bacteria was washed twice with PBS and removed. Cells were further incubated at 32ºC for 14 hours. For cell death assays (Sytox Green uptake) cells were seeded in μ-Slide 8 well glass bottom (IBIDI) at a density of $1 \cdot 10^5$ cells/well and infections were performed for 6 hours. LDH assay was performed 16 hours after infection using $5 \cdot 10^4$ cells following manufacturer instructions (Pierce LDH Cytotoxicity Assay Kit, Thermo Scientific).

For coating experiments 100 ul of a 100 cfu/nl bacterial suspension was incubated for 2 hours in 1mg/ml solution of *Ec* O111:B4 LPS (Sigma), *Mmar* M gDNA, *Ec* K112 gDNA (InvivoGen), or ODN2395 (InvivoGen) previously cell infection. After profusely washed the bacterial suspensions cells were infected. A bacterial suspension sample was taken to perform a staining using SytoxGreen and visualize the coating efficiency. *Mmar* gDNA was isolated and endotoxin-cleaned using established protocols (Ma et al 2012; Kumar et al., 2016).

mRNA synthesis

For *caspa*, *caspb*, *Casp1* and *Casp11* retrotranscription we used mMessage mMachine T7 Ultra (Invitrogen) following kit instructions. Genes were amplified using specific primers: T7 Caspa F: 5´-taatacgactcactatagggagagaatggccaaatctatcaagga-3´, Caspa R: 5´-tcagagtccggggaacagg-3´, T7 Caspb F: 5´-taatacgactcactatagggagaatggaggatattacccagct-3´, Caspb R: 5´-tcacagtccaggaaacaggta-3´, T1 Casp1 F: 5´-taatacgactcactatagggagaatggctgacaagatcctgag-3´, Casp1 R: 5´-ttaatgtcccgggaagaggt-3´, T7 Casp11 F:5´-taatacgactcactatagggagaatggctgaaaacaaacaccct-3´, Casp11 R: 5´-tgagttgccaggaaagaggt-3´. For overexpression experiments, 150 pg of mRNA were microinjected into the cell of a 1-cell stage zebrafish egg.

Western Blotting

Cells were lysed in 1x RIPA buffer (Cell Signaling) with protease inhibitors (Roche), resolved on a 12.5% SDS-PAGE precast gel (BioRad) and transferred onto a 0.2 um PVDF membrane (BioRad). The membrane was blocked with 5% v/v milk in TBS buffer at room temperature for 2 h. The immunodetection was conducted by incubating the membrane with the anti-Casp11 antibodies (1:1000, Abcam), anti-GSDMD (1:1000, Abcam), anti-Actin (1:1000, Cell Signaling) for 12 h at 4° C under slow stirring. The membrane was then incubated with the secondary antibody conjugated to horseradish

peroxidase (1:1000) for 2 h at RT. Target proteins were visualized by chemiluminiscence using the Clarity Western ECL Substrate (BioRad).

Sytox Green cell uptake

Impermeable Sytox Green Nucleic Acid Stain (ThermoFisher Scientific) was used at a final concentration of 5 µM to quantify cell death in Raw264.7 macrophages.

FLICA staining

FAM-YVAD-FMK or 660-YVAD-FMK FLICA Caspase-1 Assay Kits (ImmunoChemistry Technologies) were used for zebrafish Caspa detection. The probe was diluted in egg water (1:200) and larvae were incubated during 1´5 hours at 28ºC. Larvae were profusely washed in egg water before *in vivo* imaging.

***Mmar* culture DNA staining**

Bacterial cultures were incubated O/N in a 5 µM solution of Draq5 Fluorescent Probe Solution (ThermoFisher Scientific). Bacterial suspensions were washed 3 times with PBS before the cells were infected.

TUNEL assay

PFA fixed zebrafish larvae were used in combination with the *In situ* Cell Death Detection Kit (TMR and Fluorescein) (Roche). After O/N fixation larvae were washed and permeabilized for 45 min at 37ºC using Proteinase K. TUNEL reactions were performed at 37ºC O/N.

Caspase-1 activity assay

Caspase-1 activity was assayed using the fluorometric substrate Z-YVAD-AFC (Santa Cruz) as described previously (Tyrkalska et al., 2016). The fluorescence was measured in a Infinite M1000 microplate reader (Tecan) at an excitation wavelength of 400 nm and an emission wavelength of 505 nm.

LysoTracker staining

Zebrafish larvae were immersed in egg water containing 10 µM LysoTracker Red DND-99 solution (ThermoFisher Scientific) for 1 hour. Before mounting and imaging larvae were washed 3 times with egg water.

Lentiviral shRNA generation

shRNA's were acquired from the Mission library (Sigma, Zwijndrecht, the Netherlands) and were kindly provided by (dept. of Virus and Stem Cell Biology, LUMC, Leiden). For each gene 3 clones were selected for subsequent selection of the 2 most potent knock-downs for each gene.

Low passage (between 4 and 12) Hek293T cells (ATCC, USA) were seeded to 30% confluency in a 75cm^2 culture vessel one day prior to transfection. For the assembly of lentiviral particles co-transfection of virulence and packaging vectors (pMD2.G (Addgene no. #12259) and psPAX (Addgene no. #12260)) with final concentrations of 0,72 pmol, 1,3pmol and 1,64pmol for virulence, packaging and shRNA plasmids respectively. Plasmids and liposomal transfectant lipoD293 (Signagen, Rockville, USA) were mixed in separate 500µL volumes of DMEM-F12 without fetal calf serum (FCS; Gibco, Landsmeer, The Netherlands), with a final concentration of lipoD293 was 3% (v/v). The separate volumes were thoroughly mixed and allowed to complex for 30 min. The liposomal complex was added drop wise to the medium of the HEK293T cells, where after the cells were incubated for 24 h to allow for efficient transfection.

After 24 hours the medium was replaced with 20 ml and the culture was incubated for 3 days. Viral particles were harvested through subsequent collection of the culture supernatant and were purified through filtration over a 0,2µm low protein binding PES membrane filter (Millex, Amsterdam, The Netherlands). Lentiviral supernatant was aliquoted and kept at -80°C prior to use. Lentiviral titer was determined using the Lentivirus-Associated p24 ELISA Kit (Cell biolabs, San Diego, USA) as per the supplier instructions.

Raw264.7 macrophage cultures (ATCC) were maintained in DMEM-F12 containing 10% FCS, and were cultured up to passage 15. Low passage Raw264.7 cells were seeded to 20% confluency in 25cm^2 culture vessels and were left to adhere overnight, the cells were subsequently transduced with 4 multiplicity of infection (MOI) scrambled control shRNA containing lentiviral particles or 4 MOI of targeting shRNA containing viral particles in medium supplemented with 8 µg/ml DEAE-dextran (Sigma). Medium was exchanged after 24 hours and puromycin (Gibco) selection (1,5µg/ml) was started 48 hours post transfection. After two passages (one week) under puromycin selection the remaining resistant clones were assessed for knock down efficacy. Knock down efficacy was assessed by qPCR using the following primers: GSDMD F: 5´- catcggcctttgagaaagtg-3´, GSDMD R: 5´- tcctgttcagaaggcagtag-3´, CASP11 F: 5´- tggaagctgatgctgtcaag-3´, CASP11 R: 5´- agcctcctgttttgtctgc-3´, GAPDH F: 5´- atggtgaaggtcggtgtga-3´, GAPDH R: 5´- ctggaacatgtagaccatgt-3´-

Microscopy

Zebrafish larvae were imaged using a MZ16FA stereo fluorescence microscopy with DFC420C camera (Leica). Confocal z-tacks of zebrafish larvae and cell cultures were obtained on a TCS SP8 (Leica) using a 40x oil-immersion objective (NA 1.30). Images were processed and quantified using QuantiFish (http://doi.org/10.5281/zenodo.1182791) for stereo images or Fiji (Schindelin et al., 2012) for confocal images.

Statistical Analysis

Statistical analysis was performed using GraphPad Prism 6 program (GraphPad Software). Comparisons between two groups were done using Mann-Whitney test. For analyzing differences between multiple groups ordinary one-way ANOVA + Tukey´s multiple comparisons test was used. Statistical significance was defined as *$p<0.05$, **$p<0.01$, ***$p<0.001$, ****$p<0.0001$.

SUPPLEMENTAL INFORMATION

Supplemental information includes 6 figures.

ACKNOWLEDGMENTS

We thank other members of the Meijer Laboratory for helpful discussions. We also thank fish facility and microscope facility staff at Leiden Institute of Biology. We thank Dr. Sander van Kasteren for kindly providing Raw264.7 macrophages and Martijn Rablink for kindly providing shRNA plasmids. The work was funded by grant H2020-MSCA-IF-2014-655424 (M.V) from the European H2020 Marie Skłodowska-Curie Intra-European Fellowship program.

AUTHOR CONTRIBUTIONS

Conceptualization M.V and A.H.M.; Formal Analysis M.V. and A.H.M.; Investigation M.V.; Resources M.vd.V., A.G., M.L.; Writing – Original Draft M.V. and A.H.M.; Writing – Review & Editing M.V., M.vd.V., A.G. and A.H.M.; Visualization M.V.; Funding Acquisition M.V. and A.H.M.

REFERENCES

Afonina, I.S., Müller, C., Martin, S.J. and Beyaert, R. (2015). Proteolytic processing of Interleukin-1 Family Cytokines: Variations on a Common Theme. Immunity 42(6), 991-1004.

Baroja-Mazo, A., Martín-Sanchez, F., Gomez, A.I., Martinez, C.M., Amores-Iniesta, J., Compan, V., Barbera-Cremades, M., Yagüe, J., Ruiz-Ortiz, E., Anton, J., Buján, S., Couillin, I., Brough, D., Arostegui, J.I. and Pelegrín, P. (2014). The NLRP3 inflammasome is released as a particulate danger signal that amplifies the inflammatory response. Nat Immunol 15, 738–748.

Basabara, R.J. (2008). Experimental tuberculosis: the role of comparative pathology in the discovery of improved tuberculosis treatment strategies. Tuberculosis 88, S35–S47. doi: 10.1016/S1472-9792(08)70035-0.

Benard, E.L., van der Sar, A.M., Ellett, F., Lieschke, G.J., Spaink, H.P. and Meijer, A.H. (2012). Infection of zebrafish embryos with intracelular bacterial pathogens. J Vis Exp 61, pii:3781.

Bohrer, A.C., Tocheny, C., Assmann, M., Ganusov, V.V. and Mayer-Barber, K.D. (2018). Cutting Edge: IL-1R1 Mediates Host Resistance to Mycobacterium tuberculosis by Trans-Protection of Infected Cells. J Immunol. 201(6):1645-1650. doi: 10.4049/jimmunol.1800438.

Broz, P. and Dixit, V. (2016). Inflammasomes: mechanism of assembly, regulation and signalling. Nat Rev Immunol 16(7), 407-420.

Cadena, A.M., Fortune, S.M. and Flynn, J.L. (2017). Heterogeneity in tuberculosis. Nat Rev Immunol 17,691-702).

Cohen, S.B., Gern, B.H., Delahaye, J.L., Adams, K.N., Plumlee, C.R., Winkler, J.K., Sherman, D.R., Gerner, M.Y. and Urdahl, K.B. (2018). Alveolar Macrophages Provide an Early Mycobacterium tuberculosis Niche and Initiate Dissemination. Cell Host Microbe 24(3), 439-446. doi: 10.1016/j.chom.2018.08.001.

Cronan, M.R., Beerman, R.W., Rosenberg, A.F., Saelens, J.W:, Johnson, M.G., Oehlers, S.H., Sisk, D.M., Smith, K.L.J., Medvitz, N.A., Miller, S.E., Trinh, L.A., Fraser, S.E., Madden, J.F., Turner, J., Stout, J.E., Lee, S. and Tobin, D.M. (2016) Macrophage epitelial reprograming underlies mycobacterial granuloma formation and promotes infection. Immunity 45(4), 861-876.

Davis J.M., Clay H., Lewis J.L., Ghori N., Herbomel P. and Ramakrishnan L. (2002). Real-time visualization of mycobacterium-macrophage interactions leading to initiation of granuloma formation in zebrafish embryos.Immunity 17, 693-702.

Davis, J.M. and Ramakrishnan, L. (2009). The role of the granuloma in expansión and dissemination of early tuberculosis infection. Cell 136(1), 37-49.

Evavold, C.L., Ruan, J., Tan, Y., Xia, S., Wu, H. and Kagan, J.C. (2018). The pore-forming protein Gasdermin D regulates interleukin-1 secretion from living macrophages. Immunity 48(1), 35-44.

Fais, S. (2007). Cannibalism: a way to feed on metastatic tumors. Cancer Lett 258(2), 155-164.

Fais, S. and Overholtzer, M. (2018). Cell-in-cell phenomena in cancer. Nat Rev Cancer 18(12), 758-766.

Flemming, H.C., Wingender, J., Szewzyk, U., Steinberg, P., Rice, S.A. and Kjlleberg, S. (2016). Biofilms: an emergent form of bacterial life. Nat Rev Microbiol 14(9), 563-575.

Franklin, B.S., Bossaller, L., De Nardo, D., Ratter, J.M., Stutz, A., Engels, G., Brenker, C., Nordhoff, M., Mirandola, S.R., Al-Amoudi, A., Mangan, M.S., Zimmer, S., Monks, B.G., Fricke, M., Schmidt, R.E., Espevik, T., Jones, B., Jamicki, A.G., Hansbro, P.M., Busto, P., Marshak-Rothstein, A., Homemann, S., Aguzzi, A., Kastenmüller, W. And Latz, E. (2014). The adaptor ASC has extracellular and 'prionoid' activities that propagate inflammation. Nat. Immunol. 15, 727–737.

Garanina, A.S., Khashba, L.A. and Onishchenko, G.E. (2015). Stages of cell cannibalism –entosis- in normal human keratinocyte culture. Biochemistry 80 (11), 1469.1477. doi: 10.1134/S0006297915110085.

Grosset, J. (2003). Mycobacterium tuberculosis in the extracellular compartment: an underestimated adversary. Antimicrob Agents Chemother 47(3), 833-836. doi:10.1128/AAC.47.3.833-836.2003

Hamann, J.C., Surcel, A., Chen, R., Teragawa, C., Albeck, J.G., Robinson, D.N. and Overholtzer, M. (2017). Entosis Is Induced by Glucose Starvation. Cell Rep 20(1), 201-210.

Ibañez de Aldecoa, A., Zafra, O. and González-Pastor, J.E. (2017). Mechanisms and regulation of extracellular DNA release and its biological roles in microbial communities. Front Microbiol 8, 1390.

Kayagaki , N., Stowe, I.B., Lee, B.L., O´Rourke, K., Anderson, K., Warming, S., Cuellar, T., Haley, B., Roose-Girma, M., Phung, Q.T., Liu, P.S., Lill, J.R., Li, H., Wu, J., Kummerfeld, S., Zhang, J., Lee, W.P., Snipas, S.J., Salvesen, G.S., Morris, L.X., Fitzgerald, L., Zhang, Y., Bertram, E.M., Goodnow, C.C. and Dixit, V.M. (2015). Caspase-11 cleaves gasdermin D for non-canonical inflammasome signaling. Nature 526(7575), 666-671.

Kayagaki, N., Warming, S., Lamkanfi, M., Vande Walle, L., Louie, S., Dong, J., Newton, K., Qu, Y., Liu, J., Heldens, S., Zhang, J., Lee, W.P., Roose-Girma, M. and

Dixit, V.M. (2011). Non-canonical inflammasome activation targets caspase-11. Nature 479(7371), 117–121.

Krishna, S. and Overholtzer, M. (2016). Mechanisms and consequences of entosis. Cell Mol Life Sci 73(11-12), 2379-2386.

Kumar, P., Marathe, S. and Bhaskar, S. (2016). Isolation of genomic DNA from Mycobacterium species. Bio-protocol 6(5), e1751.

Kuri, P., Schieber, N.L., Thumberger, T., Wittbrodt, J., Schawab, Y. and Leptin, M. (2017). Dynamics of in vivo ASC speck formation. J Cell Biol 216(9), 2891-2909.

Lee, J., Repasy, T., Papavinasasundaram, K., Sassetti, C. and Komfield, H. (2011). Mycobacterium tuberculosis induces an atypical cell death mode to escape from infected macrophages. PLoS One 6(3), e18367.

Lerner, T.R., Borel, S. and Gutierrez, M.G. (2015). The innate immune response in human tuberculosis. Cell Microbiol 17(9), 1277-1285.

Liu, C.H., Liu, H. and Ge, B (2017). Innate immunity in tuberculosis: host defense vs pathogen evasión. Cell Mol Immunol 14(12), 963-975.

Ma, R., Zhao, J., Du, H.C., Tian, S. and Li, L.W. (2012). Removing endotoxin from plasmid samples by Triton X-114 isothermal extraction. Anal Biochem 424(2), 124-126.

Man, S.M., Karki, R. and Kanneganti, T.D. (2017). Molecular mechanisms and functions of pyroptosis, inflammatory caspases and inflammasomes in infectious diseases. Immunol Rev 277(1), 61-75.

Man, S.M., Place, D.E., Kuriakose, T. and Kanneganti, T.D. (2017). Inferferon-inducible-guanylate-binding proteins at the interface of cell-autonomous immunity and inflammasome activation. J Leukoc Biol 101(1), 143-150.

Manzanillo, P.S., Shiloh, M.U., Portnoy, D.A. and Cox, J.S. (2012). Mycobacterium tuberculosis activates the DNA-dependent cytosolic surveillance pathway within macrophages. Cell Host Microbe 11, 469–480.

Marakalala, M. J., Raju, R. M., Sharma, K., Zhang, Y. J., Eugenin, E. A., Prideaux, B., Daudelin, I.B., Chen, P.Y., Booty, M.G., Kim, J.H., Eum, S.Y., Via, L.E., Behar, S.M., Barry, C.E., Mann, M., Dartois, V. and Rubin, E.J. (2016). Inflammatory signaling in human tuberculosis granulomas is spatially organized. Nat. Med. 22, 531–538. doi: 10.1038/nm.4073

Martinon, F., Burns, K. and Tschopp, J. (2002). The inflammasome: a molecular platform triggering activation of inflammatory caspases and processing of proIL-beta. Mol Cell 10, 417–426.

Masumoto, J., Zhou, W., Chen, F.F., Su, F., Kuwada, J.Y., Hidaka, E., Katsuyama, T., Sagara, J., Taniguchi, S., Ngo-Hazelett, P., Postlethwait, J.H., Núñez, G. and Inihara, N. (2003). Caspy, a zebrafish Caspase, activated by ASC oligomerization is required for pharyngeal arch development. J Biol Chem 278(6), 4268-4276.

Mayer-Barber, K.D., Andrade, B.B., Barber, D.L., Hieny, S., Feng, C.G., Caspar, P., Oland, S., Gordon, S. and Sher, A. (2011). Innate and adaptive interferons suppress IL-1a and IL-1b production by distinct pulmonary myeloid subsets during Mycobacterium tuberculosis infection. Immunity 35(6), 1023-1034.

Mayer-Barber, K.D., Barber, D.L., Shenderov, K., White, S.D., Wilson, M.S., Cheever, A., Kugler, D., Hieny, S., Caspar, P., Núñez, G., Schlueter, D., Flavell, R.A., Sutterwala, F.S. and Sher, A. (2010). Caspase-1 independent IL-1beta production is critical for host resistance to mycobacterium tuberculosis and does not require TLR signaling in vivo. J immunol 184(7), 3326-3330.

McClean, C.M. and Tobin, D.M. (2016). Macrophage form, function, and phenotype in mycobacterial infection: lessons from tuberculosis and other diseases. Pathog Dis 74(7), pii:ftw068. Doi:10.1093/femspd/ftw068.

Meijer, A.H. (2016). Protection and pathology in TB: learning from the zebrafish model. Semin Immunopathol 38(2), 261-273.

Miao, E.A., Rajan, J.V. and Aderem, A. (2011). Caspase-1-induced pyroptotic cell death. Immunol 243, 206–214.

Monteleone, M., Stanley, A.C., Chen, K.W., Brown, D.L., Bezbradica, J.S., von Pein, J.B., Holley, C.L., Boucher, D., Shakespear, M.R., Kapetanovic, R., Rolfes, V., Sweet, M.J., Stow, J.L. and Schroder, K. (2018). Interleukin-1β Maturation Triggers Its Relocation to the Plasma Membrane for Gasdermin-D-Dependent and -Independent Secretion. Cell Rep 24(6), 1425-1433.

Ni, C., Che, Y., Zeng, M., Pei, R., Du, Y., Tang, L., Wang, M., Hu, Y., Zhu, H., He, M., Wei, X., Wang, S., Ning, X., Wang, M., Wang, J., Ma, L., Chen, X., Sun, Q., Tang, H., Wang, Y. And Wang, X. (2015). In-Cell infection: a novel pathway for Epstein-Barr virus infection mediated by cell-in-cell structures. Cell Res 25(7): 785-800.

Ogryzko, N.V., Hoggett, E.E., Solaymani-Kohal, S., Tazzyman, S., Chico, T.J., Renshaw, S.A. and Wilson, H.L. Zebrafish tissue injury causes upregulation of interleukin-1 and caspase-dependent amplification of the inflammatory response. Dis Model Mech 7(2), 259-264.

Overholtzer, M. and Brugge, J.S. (2008). The cell biology of cell-in-cell structures. Nat Rev Mol Cell Biol 9(10), 796-809.

Overholtzer, M., Mailleux, A.A., Mouneimne, G., Normand, G., Schnitt, S.J., King, R.W., Cibas, E.S. and Brugge, J.S. (2007). A nonapoptotic cell death process, entosis, that occurs by cell-in-cell invasion. Cell 131, 966-979. doi:10.1016/j.cell.2007.10.040.

Pagan, A.J. and Ramakrishnan, L. (2018). The formation and function of granulomas. Annu Rev Immunol 36, 639-665.

Pagán, A.J., Yang, C.T., Cameron, J., Swaim, L.E., Ellett, F., Lieschke, G.J. and Ramakrishnan, L. (2015). Myeloid growth factors promote resistence to mycobacterial infection by curtailing granuloma necrosis through macrophage replenishment. Cell Host Microbe 18(1), 15-26.

Palazón-Riquelme, P. and Lopez-Castejon, G. (2018). The inflammasomes, immune guardians at defence barriers. Immunology 155(3), 320-330.

Pelegrin, P., Barroso-Gutierrez, C. And Surprenant, A. (2008). P2X7 receptor differentially couples to distinct reléase pathways for IL-1 in mouse macrophage. J Immunol 180(11), 7147-7157.

Ramakrishnan, L. (2012) Revisiting the role of the granuloma in tuberculosis.Nat Rev Immunol 12, 352-366.

Roca, F.J. and Ramakrishnan, L. (2013). TNF dually mediates resistence and susceptibility to mycobacteria via mitocondrial reactive oxygen species. Cell 153(3), 521-534.

Russo, A.J., Behl, B. Banerjee, I. and Rathinam, V.A.K. (2018). Emerging insights into noncanonical inflammasome recognition of microbes. J Mol Biol 430(2), 207-216.

Santos, J.C., Dick, M.S., Lagrange, B., Degrandi, D., Pfeffer, K., Yamamoto, M., Meunier, E., Pelczar, P., Henry, T. and Broz, P. (2017). LPS targets host guanylate-binding proteins to the bacterial outer membrane for non-canonical inflammasome activation. EMBO J 37(6), pi:e98089.

Shi, J., Gao, W. and Shao, F. (2017). Pyroptosis: gasdermin-mediated programmed necrotic cell death. Trends Biochem Sci 42(4), 245-254.

Shi, J., Zhao, Y., Wang, K., Shi, X., Wang, Y., Huang, H., Zhuang, Y., Cai, T., Wang, F. and Shao, F. (2015). Cleavage of GSDMD by inflammatory caspases determines pyroptotic cell death. Nature 526(7575), 660-665.

Shi, J., Zhao, Y., Wang, Y., Gao, W., Ding, J., Li, P., Hu, L. and Shao, F. (2014). Inflammatory caspases are innate immune receptors for intracellular LPS. Nature. 2014;514:187–92.

Schindelin, J., Arganda-Carreras, I., Frise, E., Kaynig, V., Longair, M., Pietzsch, T., Preibisch, S., Rueden, C., Saalfeld, S., Schmid, B., Tinevez, J.Y., White, D.J.,

Hartenstein, V., Eliceiri, K., Tomancak, P. and Cardona, A. (2012). Fiji: an open-source platform for biological-image analysis. Nat Methods 9(7), 676-682.

Sia, J.K., Georgieva, M. And Rengarajan, J. (2015). Innate immune defenses in human tuberculosis: an overview of the interactions between mycobacterium tuberculosis and innate immune cells. J Immunol Res 2015, 747543.

Sokolovska, A., Becker, C.E., Ip W.K.E. ,Rathinam V.A.K. ,Brudner M. ,Paquette N. ,Tanne A. ,Vanaja S.K. , Moore K.J. , Fitzgerald K.A., Lacy-Hulbert, A. and Stuart, L.M. (2013). Activation of caspase-1 by the NLRP3 inflammasome regulates the NADPH oxidase NOX2 to control phagosome function. Nat Immunol 14 (6), 543-553.

Stanley, S.A., Johndrow, J.E., Manzanillo, P. and Cox, J.S. (2007). The type I IFN response to infection with Mycobacterium tuberculosis requires ESX-1-mediated secretion and contributes to pathogenesis. J Immunol 178, 3143–3152.

Sun, Q., Cibes, E.S., Huang, H., Hodgson, L. and Overholtzer, M. (2014). Induction of entosis by epithelial cadherin expression. Cell Res 24(11), 1288-1298.

Tyrkalska, S.D., Candel, S., Angosto, D., Gomez-Abellán, V., Martín-Sánchez, F., García-Moreno, D., Zapata-Pérez, R., Sánchez-Ferrer, A., Sepulcre, M.P., Pelegrín, P., and Mulero, V. (2016). Neutrophils mediate Salmonela Typhimurium clearance through the GBP4 inflammasome-dependent production of prostaglandins. Nat Commun 7, 12077.

Vojtech, L.N., Scharping, N., Woodson, J.C. and Hansen, J.D. (2012). Roles of inflammatory caspases during processing of zebrafish interleukin-1beta in Francisella noatunensis infection. Infect Immun 80, 2878–2885 (2012).

Vorkapic, D., Pressier, K. and Schild, S. (2016). Multifaceted roles of extracellular DNA in bacterial physiology. Curr Genet 62(1), 71-79.

Yang, J., Zhao, Y. And Shao, F. (2015). Non-canonical activation of inflammatory caspases by cytosolic LPS in innate immunity. Curr. Opin. Immunol 32, 78–83.

Yang, Y.Q. and Li, J.C. (2012). Progress of research in cell-in-cell phenomena. Anat Rec (Hoboken) 295(3), 372-377.

FIGURE 1

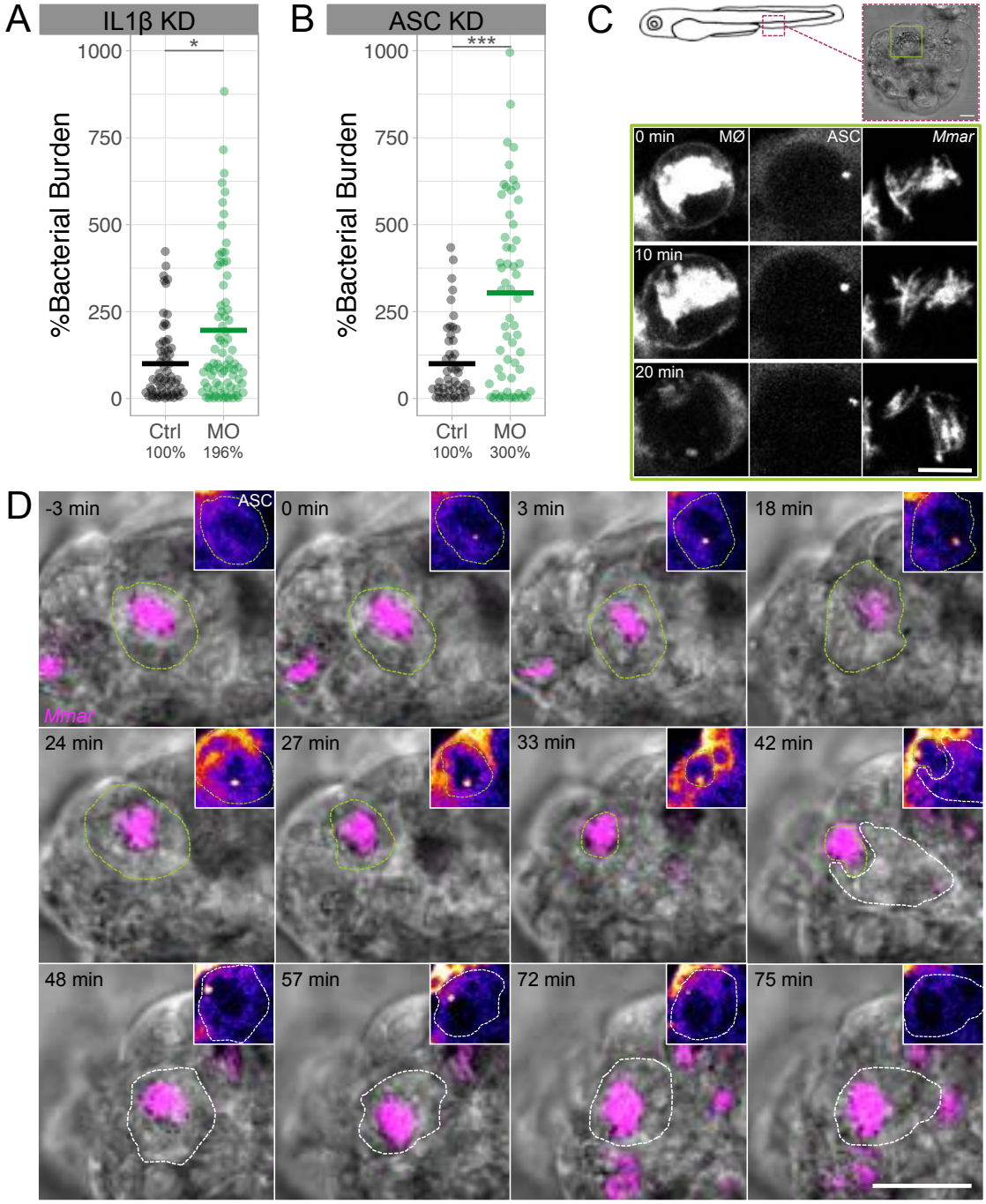

Figure 1. Asc and Il1b are host-beneficial during *Mmar* infection in zebrafish. (A, B) Bacterial burden data after transient knockdown (KD) with *il1β* or *asc* morpholinos (MO) at 2 days post-infection (dpi) (300 cfu). (C) Bright field (BF) and *in vivo* time-lapse confocal images of Asc speck-dependent pyroptosis of a *mpeg1*:mCherry labelled macrophage (MØ) in zebrafish granuloma at 3dpi. (D) *In vivo* confocal images showing Asc speck formation in Cell 1 (green dotted line) and degradation by Cell 2 (white dotted line) after phagocytosis (Movie 1). Insets show Asc-GFP protein (Fire LUTs). Data is accumulated from 2 independent experiments and representative of at least three

independent repeats. Each data point (A, B) represents a single zebrafish larva. Mann-Whitney test (A, B), *$p<0.05$ and ***$p<0.001$. Scale bars are 10 (C) and 20 (D) μm.

FIGURE 2

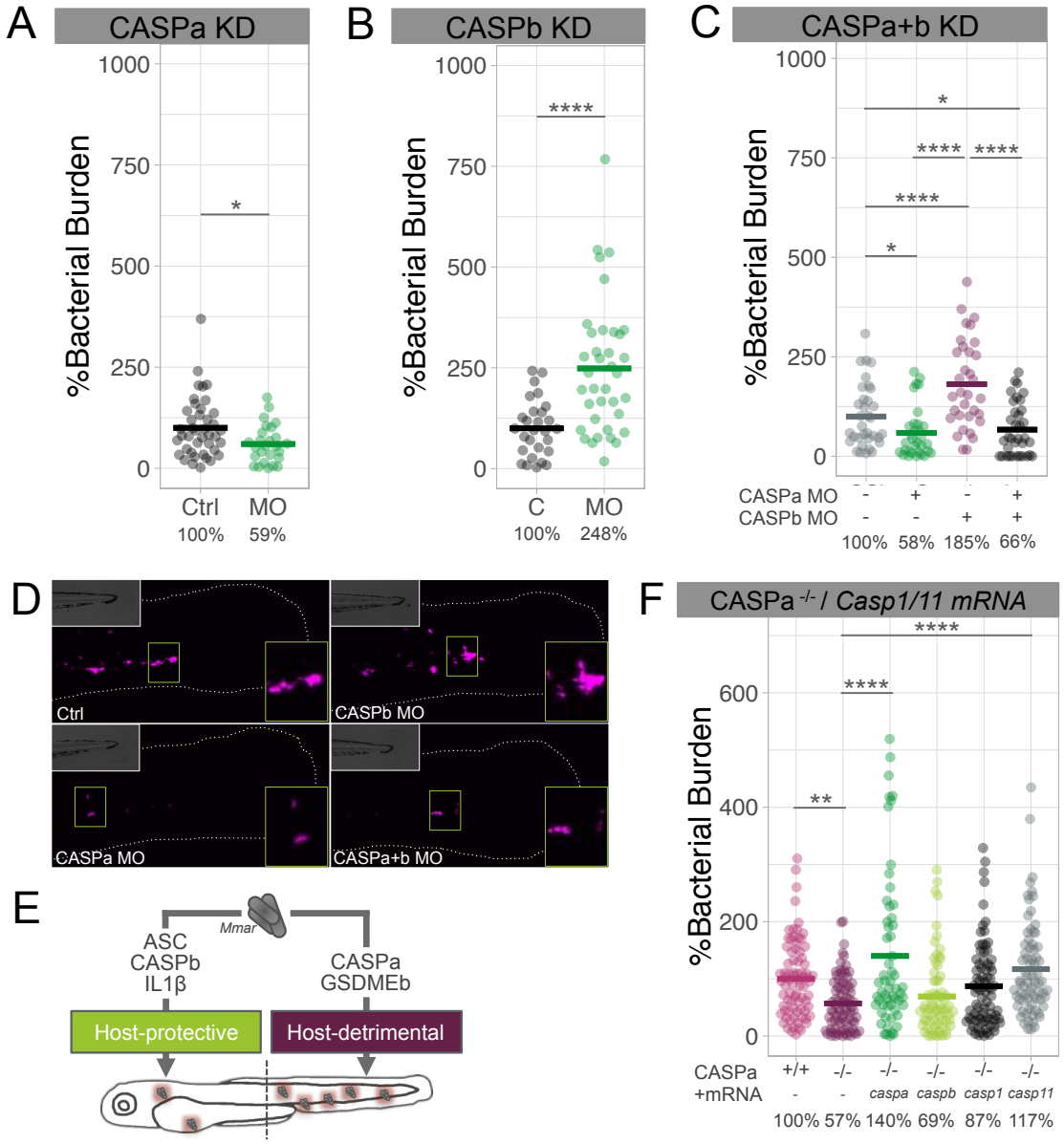

Figure 2. Two differentiated inflammasome axes are activated during *Mmar* infection (A, B, C) Bacterial burden data after transient *caspa*, *caspb* or *caspa+caspb* KD in zebrafish larvae at 2dpi (300 cfu). (D) Representative fluorescence images showing differential *Mmar* growth in zebrafish macrophages in the tail fin (outlined and BF images in insets) under different KD situations at 2dpi (300 cfu) (E) Schematic representing the two inflammasome-related axes activated during *Mmar* infection in zebrafish. (F) Bacterial burden data showing the effect of zebrafish *caspa* and *caspb* mRNAs and murine *Casp1* and *Casp11* mRNAs overexpression in *caspa*$^{-/-}$ zebrafish larvae. Data is accumulated from 2 independent experiments and representative of at least three independent repeats. Mann-Whitney test (A, B) and ordinary one-way ANOVA + Tukey´s multiple comparisons test (C, F), *p<0.05, **p<0.01, ****p<0.0001. Scale bars are 500 (D) µm.

FIGURE 3

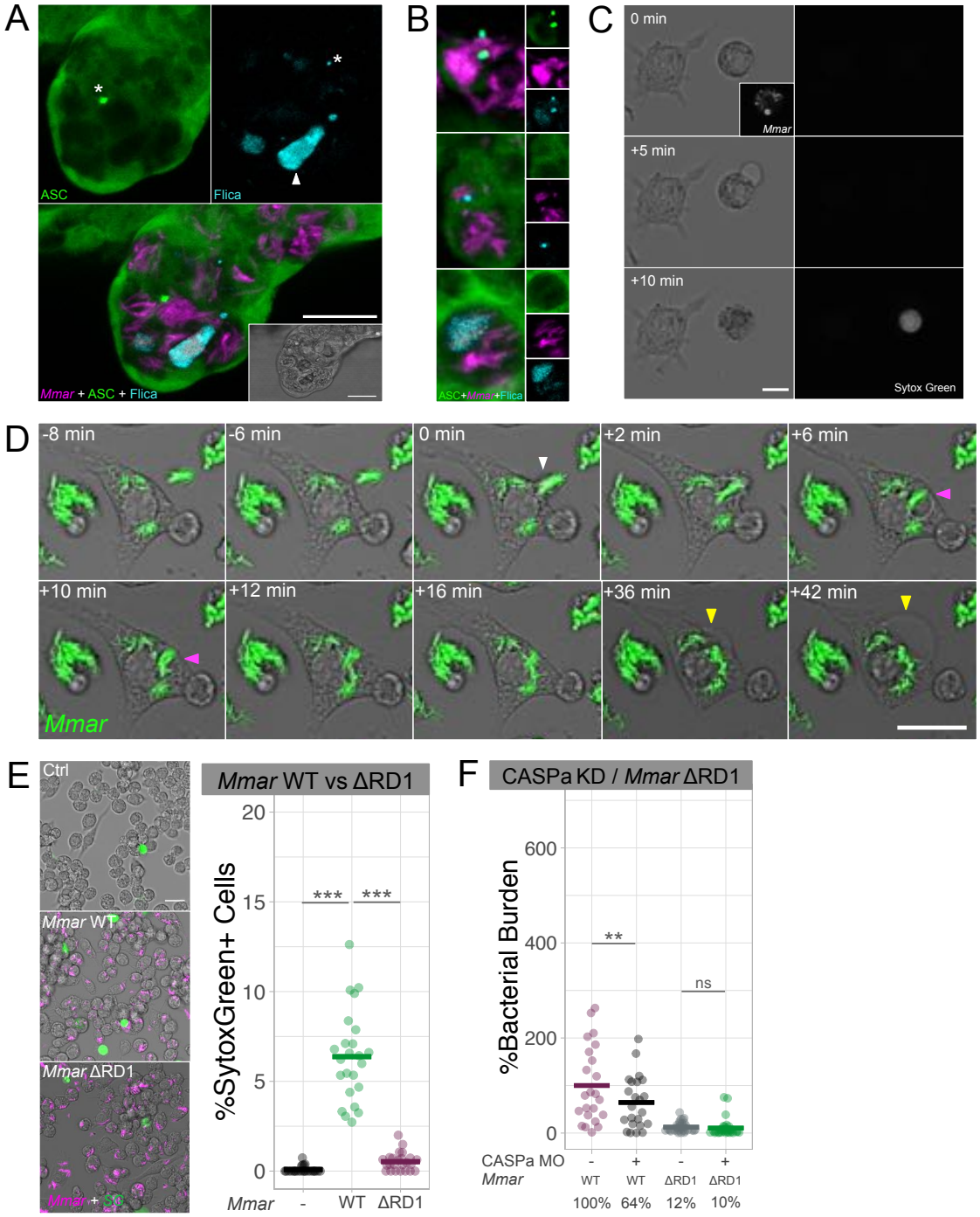

Figure 3. *Mmar* triggers ASC-independent and phagosome rupture-dependent macrophage pyroptosis. (A) Confocal images (with BF inset) of a zebrafish granuloma showing Asc and *in situ* Caspa activity at 3 dpi. Different types of specks (asterisks) and patches (arrowhead) are observed during *Mmar* infection. (B) Representative confocal images showing types of Asc/Caspa activation patterns observed during *Mmar* infections in zebrafish. (C) Confocal images showing Sytox Green (SG) uptake in ASC-deficient Raw264.7 macrophages upon *Mmar* infection (MOI 10). (D) Confocal footage showing phagocytosis (white arrowhead), phagosome formation and subsequent rupture

(magenta arrowheads) and pyroptosis (yellow arrowheads) in Raw264.7 macrophages after *Mmar* infection (MOI 10) (Movie 2). (E) Sytox Green uptake quantification in RAW264.7 macrophages at 6 hours post-infection (hpi) with *Mmar* WT and ΔRD1 (MOI 10). (F) Bacterial burden data after transient *caspa* KD in zebrafish larvae 2 days after Mmar WT and ΔRD1 infection (300 cfu). Data is representative of three independent experiments. Ordinary one-way ANOVA + Tukey´s multiple comparisons test (E, F), **$p<0.01$, ***$p<0.001$. Scale bar are 20 (A) and 10 (C, D, E) µm.

FIGURE 4

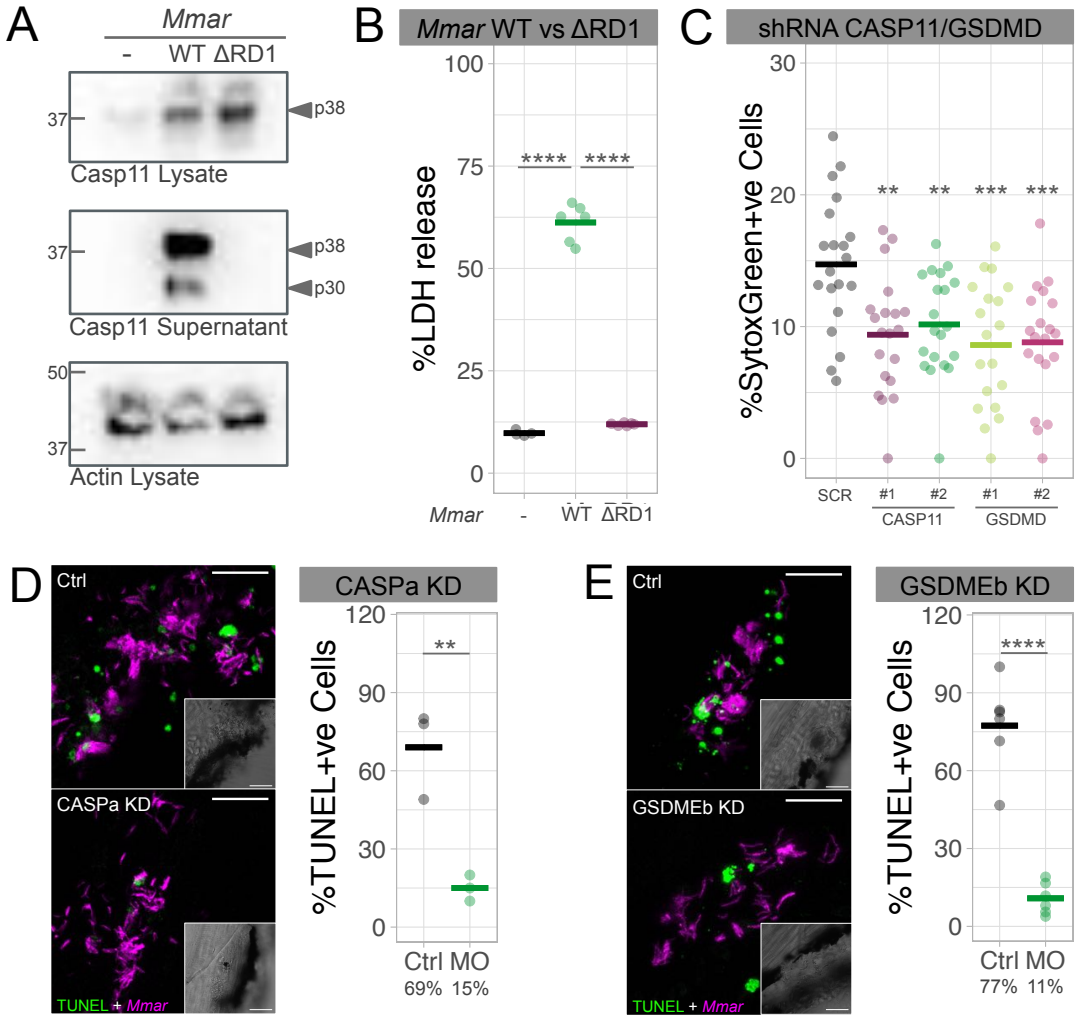

Figure 4. ***Mmar*-induced pyroptosis is CASP11/GSDMD-dependent in murine macrophages and Caspa/Gsdmeb-dependent in zebrafish larvae**. (A) Casp11 protein expression in cell lysates and supernatants of Raw264.7 macrophages after 16 hours of infection with *Mmar* WT and ΔRD1 (MOI 10). (B) LDH release in Raw264.7 macrophages infected for 16 hours with *Mmar* WT and ΔRD1 (MOI 10). (C) Cell death (Sytox Green uptake) in scramble control (SCR), *Casp11* KD (x2 different shRNAs) and *Gsdmd* KD (x2 different shRNAs) Raw264.7 macrophages after 6 hpi with *Mmar* (MOI 10). (D, E) Quantification of TUNEL-positive *Mmar*-infected cells in Ctrl and *caspa* or *gsdmd* KD zebrafish larvae at 3dpi. Data is representative of three independent experiments. Mann-Whitney test (D, E) and ordinary one-way ANOVA + Tukey´s multiple comparisons test (B, C), **p<0.01, ***p<0.001, ****p<0.0001. Scale bars are 20 (D, E) µm.

FIGURE 5

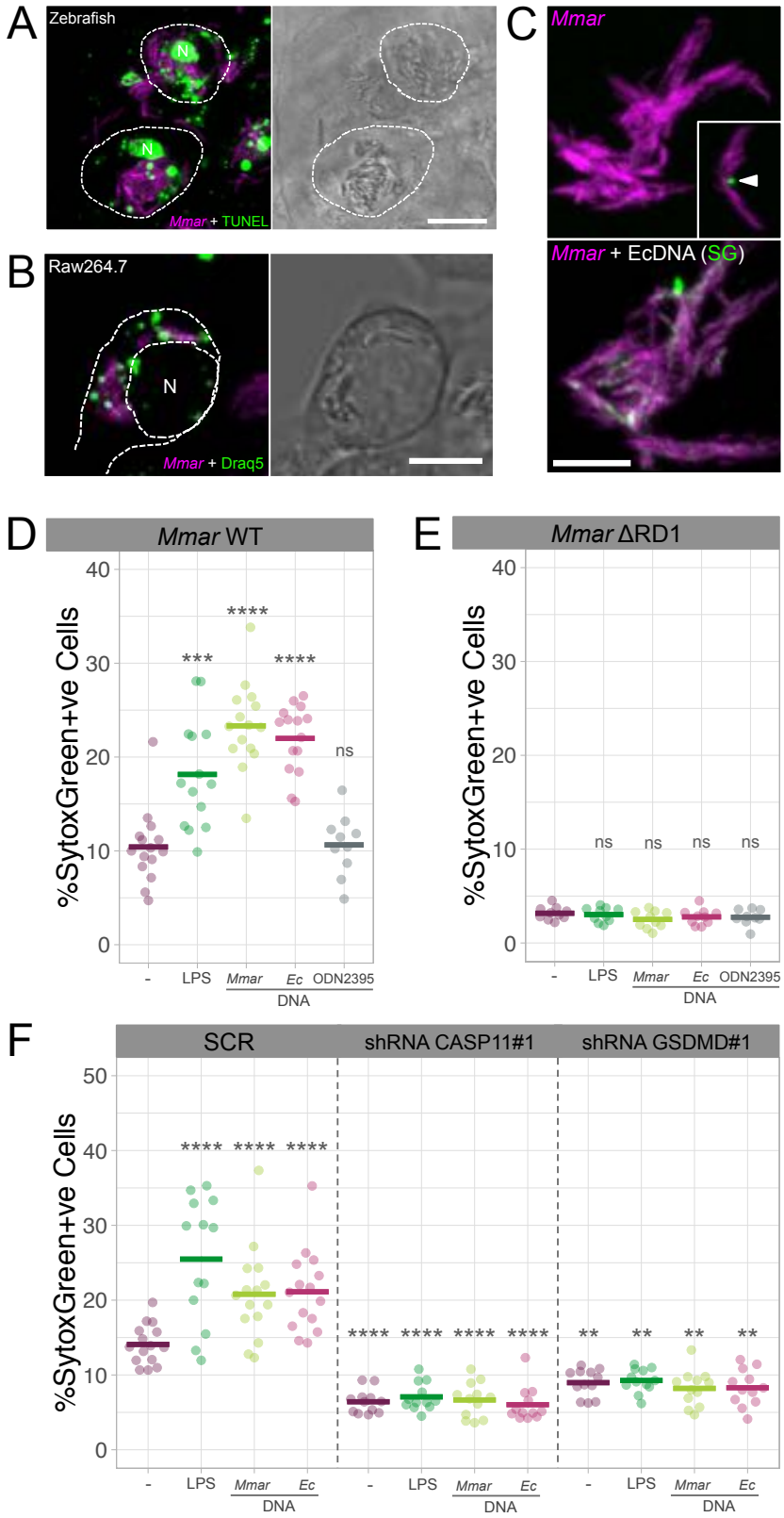

Figure 5. Extracellular *Mmar* DNA triggers CASP11/GSDMD-dependent pyroptosis. (A) Confocal images showing TUNEL-stained zebrafish cells with positive DNA signal in the nucleus (N) and around *Mmar*. (B) Confocal images of Raw264.7

macrophages infected with Draq5 (DNA) O/N-stained *Mmar* (MOI 10, 3hpi). (C) Confocal images of a *Mmar* culture incubated with Sytox Green (SG) to stain *Mmar* DNA and a *Mmar* culture incubated with *E. coli* genomic DNA and Sytox Green to visualize the DNA coating. Inset shows *Mmar* extracellular DNA. (D) Sytox Green uptake quantification in Raw264.7 macrophages infected with *Mmar* WT and *Mmar* WT coated with LPS, *Mmar* genomic DNA, *Ec* genomic DNA or ODN2395 (MOI 10, 6 hpi). (E) Sytox Green uptake quantification in Raw264.7 macrophages infected with *Mmar* ΔRD1 and *Mmar* ΔRD1 coated with LPS, *Mmar* genomic DNA, *Ec* genomic DNA or ODN2395 (MOI 10, 6hpi). (F) Sytox Green uptake quantification in SCR control, *Casp11* and *Gsdmd* shRNA Raw264.7 macrophages infected with *Mmar* WT and *Mmar* WT coated with LPS, *Mmar* genomic DNA, Ec genomic DNA or ODN2395 (MOI 10, 6hpi). Data is representative of three independent experiments. Ordinary one-way ANOVA + Tukey´s multiple comparisons test (D, E, F), **$p<0.01$, ***$p<0.001$, ****$p<0.0001$. Scale bar are 10 (A, B) and 5 (C) µm.

FIGURE 6

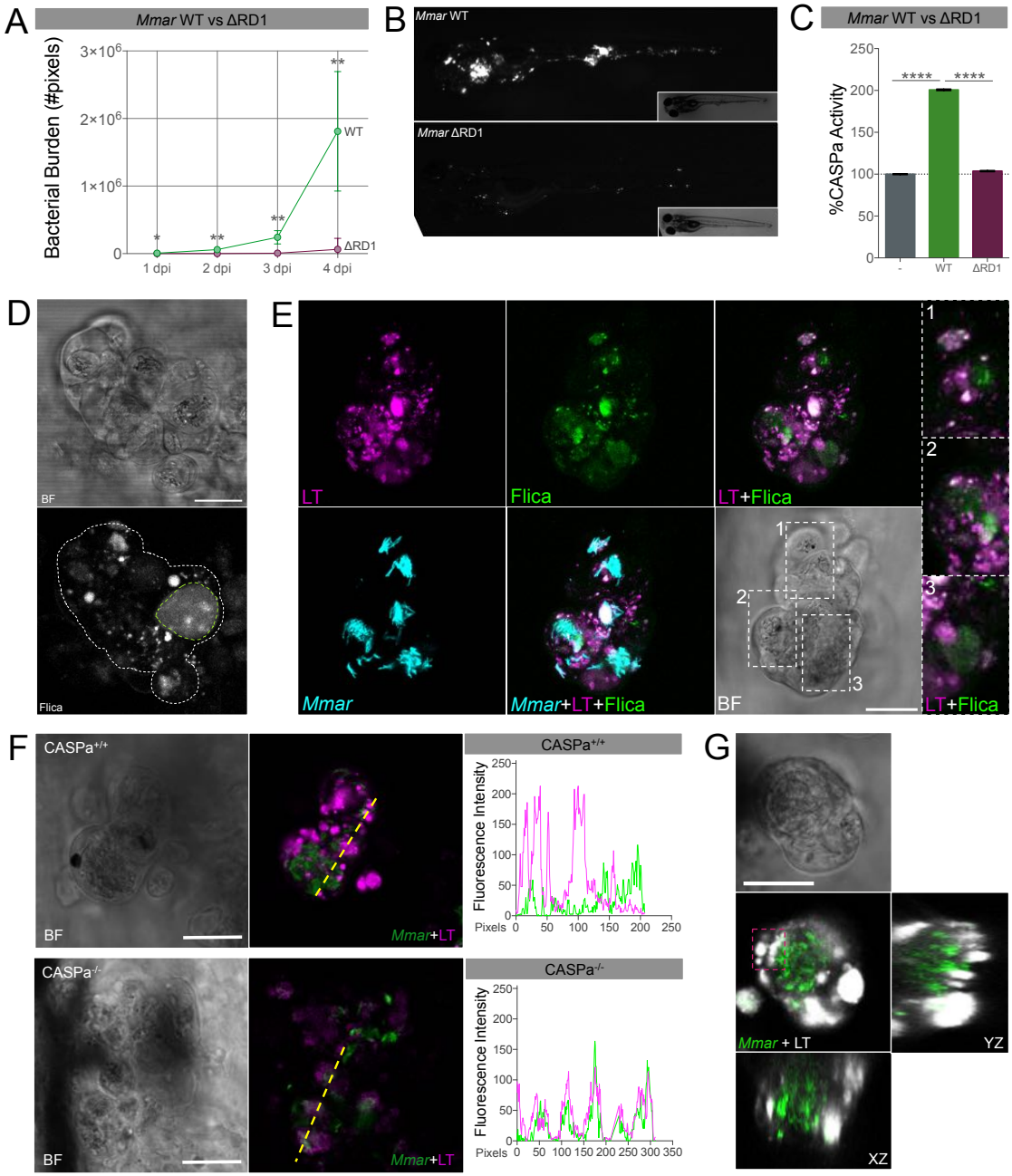

Figure 6. Caspa activation is required for the formation of granulomas in zebrafish. (A) Bacterial burden from 1 to 4 dpi after injection of 300 cfu of WT and ΔRD1 *Mmar* in zebrafish embryos. (B) Representative fluorescent images at 4dpi showing the absence of granuloma formation during *Mmar* ΔRD1 infection in zebrafish. (C) CASPa activity (YVAD-FMK) in non-infected, *Mmar* WT and *Mmar* ΔRD1-infected larvae 4 dpi (n=2, 40 zebrafish larvae/n). (D) Representative confocal images showing *in situ* CASPa activation (Flica) in a zebrafish granuloma at 3 dpi with WT *Mmar* (300 cfu). (E) Confocal images of a granuloma stained with LysoTracker (LT) and Flica. Insets 1, 2 and 3 showing Flica-positive and LT-negative phagosomes. (F) Confocal images showing the altered acidification pattern (LT) in zebrafish

granulomas due to the lack of Caspa. Fluorescence intensities of *Mmar* and LT from the yellow transects are represented on the graphs to visualize the co-localization between both markers. (G) Confocal images of LT ring-like patterns around Mmar in zebrafish granulomas (magenta square). Orthogonal views are displayed to show the lack of co-localization. Data is representative of three independent experiments. Mann-Whitney test (A) and Ordinary one-way ANOVA + Tukey´s multiple comparisons test (C), *$p<0.05$, **$p<0.01$, ****$p<0.0001$. Scale bars are 500 (B) and 20 (D, E, F, G) µm.

FIGURE 7

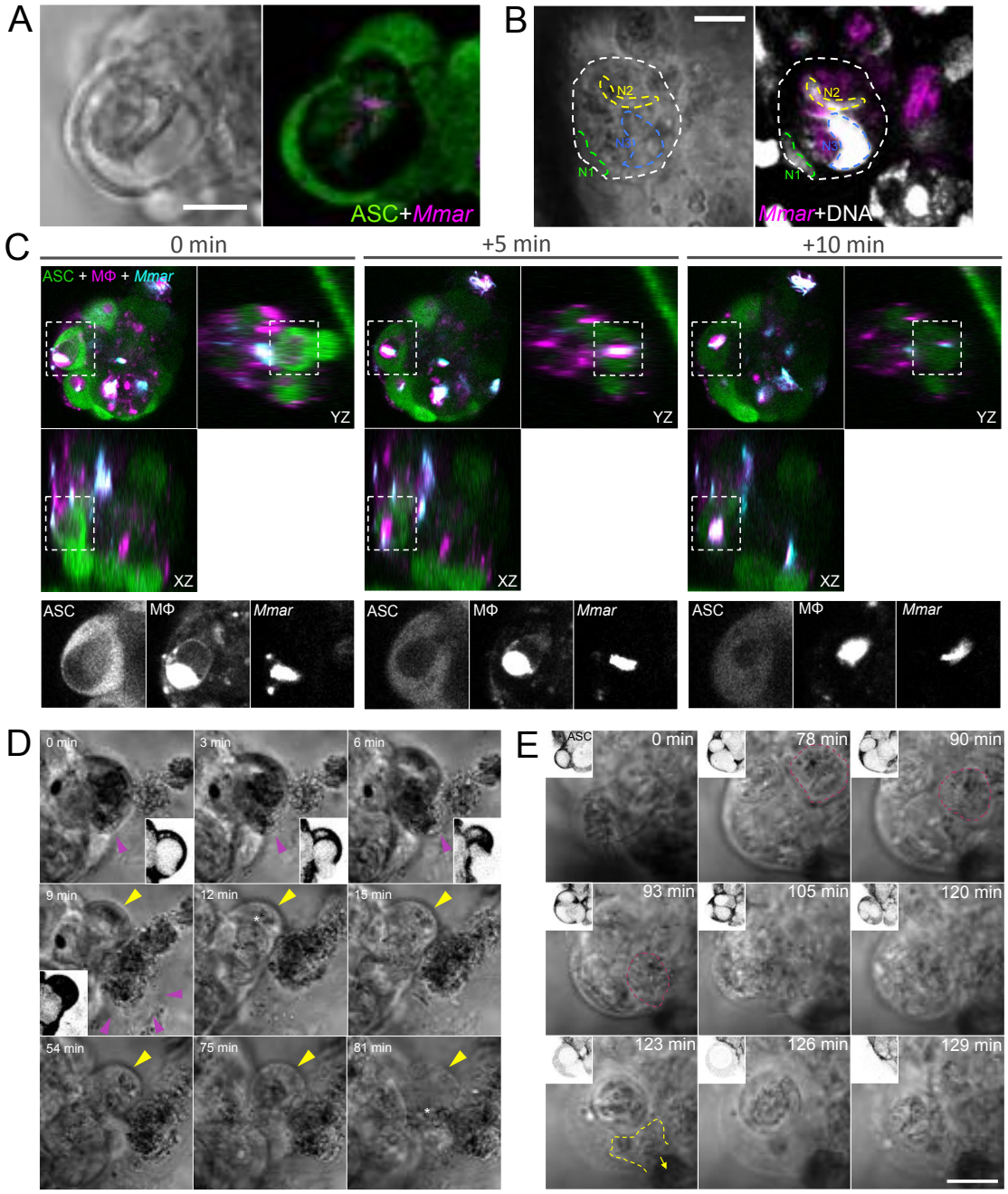

Figure 7. After cell-in-cell structure formation in granulomas, pyroptosis increases *Mmar* dissemination. (A) Confocal images of a cell-in-cell structure in a zebrafish granuloma where cytoplasmic ASC is visible in external and internal cells. (B) Confocal images showing a multinucleated cell-in-cell structure in a zebrafish granuloma. Cell 2 (N2) and cell 3 (N3), both infected, are inside Cell 1 (N1). (C) Confocal images showing the death of the internal cell (infected macrophage) in a granuloma cell-in-cell structure. Orthogonal projections are shown to facilitate the visualization of the inner cell killing. (D) Confocal images showing the release of an internal cell from the cell-in-cell structure following the initiation of pyroptotic cell death (magenta arrowheads). The infected external cell (asterisk) eventually dies via pyroptosis (yellow arrowheads)

1 hour later. Insets show Asc (inverted LUTs) for a better visualization of the process (Movie 4). (E) Confocal images showing how a single cell in a zebrafish granuloma can uptake more than 1 infected cell (outlined in BF channel). Insets show Asc (inverted LUTs) expression. Asc-independent cell death is visible in one internal and in the external cell (Movie 5). Scale bars are 10 (A, B, C, D) µm.